Simulation of Ultrasonic Lamb Wave Generation, Propagation and Detection for a Reconfigurable Air Coupled Scanner

Gordon Dobie, Andrew Spencer, Kenneth Burnham, S. Gareth Pierce, Keith Worden, Walter Galbraith, Gordon Hayward

G. Dobie, K. Burnham, S. G. Pierce, W. Galbraith and G. Hayward are with the Centre for Ultrasonic Engineering, University of Strathclyde, 204 George Street, Glasgow G1 5PJ, UK, e-mail: (see http://www.cue.ac.uk/staff.html). A. Spencer and K. Worden are with the Dynamics Research Group, University of Sheffield, Mappin Street, Sheffield, UK, S1 3JD, e-mail: (see http://www.dynamics.group.shef.ac.uk/people.html)

Abstract

A computer simulator, to facilitate the design and assessment of a reconfigurable, air-coupled ultrasonic scanner is described and evaluated. The specific scanning system comprises a team of remote sensing agents, in the form of miniature robotic platforms that can reposition non-contact Lamb wave transducers over a plate type of structure, for the purpose of non-destructive evaluation (NDE). The overall objective is to implement reconfigurable array scanning, where transmission and reception are facilitated by different sensing agents which can be organised in a variety of pulse-echo and pitch-catch configurations, with guided waves used to generate data in the form of 2-D and 3-D images. The ability to reconfigure the scanner adaptively requires an understanding of the ultrasonic wave generation, its propagation and interaction with potential defects and boundaries. Transducer behaviour has been simulated using a linear systems approximation, with wave propagation in the structure modelled using the local interaction simulation approach (LISA). Integration of the linear systems and LISA approaches are validated for use in Lamb wave scanning by comparison with both analytic techniques and more computationally intensive commercial finite element/difference codes. Starting with fundamental dispersion data, the paper goes on to describe the simulation of wave propagation and the subsequent interaction with artificial defects and plate boundaries, before presenting a theoretical image obtained from an team of sensing agents based on the current generation of sensors

and instrumentation.

Key words: Simulation, NDE, Air Coupled, Robotic, Scanner

1. Introduction

The concept of a miniature, autonomous and mobile, robotic sensor is extremely attractive for many applications involving NDE of structures. Examples include the aerospace, nuclear and petrochemical industries, where issues of scale and/or access can be paramount. In principle, such vehicles may comprise a heterogeneous fleet of remote sensing agents, each capable of operating independently, or as part of an intelligent team, combining to maximise information on the integrity of the structure under test.

Major advantages of this approach include the ability of the individual sensing agents to carry multiple sensor payloads (e.g. optical, magnetic, ultrasonic), each providing a different form of information. Provided that positional information on each mobile platform is sufficiently accurate, fusing of the individual sensor data can provide enhanced probability of defect detection. Moreover, the fleet approach has the ability to reconfigure dynamically, based upon sensor findings, or a change in operating conditions. This can take different forms. For example, a sensing agent carrying a more detailed (in terms of form and/or resolution) payload maybe 'called up' to interrogate a suspect region. Alternatively, the fleet can operate in the form of a reconfigurable array, which is capable of dynamic alteration of its shape, distribution and sensor format.

The current generation of sensing agents developed by some of the authors incorporates three inspection modalities, with each vehicle possessing visual, magnetic or ultrasonic sensor systems. Data analysis and positional control are provided via dedicated on-board processing, with inter-vehicle and base communications conducted via wireless link. Further details are contained in [1] and [2].

The creation of a fully autonomous fleet of reconfigurable sensing agents necessitates careful analysis with regard to vehicle positional accuracy, the nature of the structure under test and the optimal combination of sensor units. Arguably, this is best achieved with the aid of a computer which is capable of accurately replicating the entire system. This would also confer additional advantages for data interpretation and vehicle guidance. To be practically useful, full simulation in three dimensional (3D) space is re-

quired. This should encompass sensor behaviour (including interfacing), sensing agent positional information, structural form and defect modelling. For example, non-contact, through air ultrasound has recognised advantages for long range scanning in plate-type structures [3] [4] and is shown experimentally using sensing agent hardware in [1]. Any simulator has to be capable of modelling transducer characteristics, wave propagation and interaction with meaningful synthetic artefacts, in addition to variations in the positional certainty of individual sensing agents within the fleet. The simulator also has to be reasonably interactive, in order to assist the user with algorithmic development and system design issues.

Commercial finite element/finite difference modelling codes such as ANSYS [5], COMSOL [6] and PzFlex [7] are capable, of providing a basis for such a simulator. However, computer run-time is prohibitively expensive, especially in 3D. More approximate approaches, such as the use of ray tracing will help alleviate this problem, but invariably, modelling of the underlying physics is compromised. This paper describes an alternative approach, involving a combination of constrained sensor modelling, ray tracing and a relatively new technique, the local interaction simulation approach (LISA) [8].

This software implementation allows for relatively straightforward integration of simplified but accurate 1-D models of a piezoelectric transducer [9] with the LISA wave propagation model. Additionally, it provides a potential path for the modelling to be distributed amongst the sensing agent platforms themselves (since each sensing agent contains significant on-board computational capabilities). The overall goal is to enable structurally specific inspection tasks to be optimised taking into account both the physical aspects of the ultrasound propagation, along with the specific dynamic capabilities and restrictions of the sensing agent platforms. An additional complication is that in any optimisation task, it is vital to minimise the calculation speed for each individual propagation case considered. If the simulation time is too long, then effective optimisation (where many slightly different cases must be computed and compared) becomes very difficult. This area is one in which the advantages of the LISA simulation over conventional finite element modelling is highlighted.

The paper addresses a specific form of inspection, that of air-coupled, ultrasonic Lamb wave testing of structures. From the sensing agent standpoint, this is an important configuration. For example, both the ultrasonic transmitter and receiver can be mounted on a single sensing agent, facilitating

local pitch-catch measurements [1] [2]. Alternatively, relatively long range pulse-echo and pitch-catch scans can be performed using different spatial permutations of sensing agents, including raster, tomographic and synthetic aperture imaging formats. Importantly, the viability of using appropriate angled, air coupled (i.e. non-contact) ultrasonic transducers for generation and detection of the fundamental anti-symmetric (A0) Lamb wave and using this successfully for testing, has been demonstrated previously by some of the authors and other workers [3] [27] [11].

2. Simulation Overview

Figure 1 shows one simulation scenario detailing the generation, propagation and reception of ultrasonic Lamb waves. The sensing agent simulation provides variable transmitter and receiver positions which can be used directly as the transducer locations in the ultrasonic simulation. The simulation of mobile robots has previously been demonstrated by [12] and dynamic modelling of differential drive mobile robots is well established [13, 14, 15] and will not be detailed herein. The sensing agent model was built using the same logic and control code that is run on the computer embedded in the sensing agent [1] which talks to a common interface. When simulating a sensing agent the code is interfaced to a dynamic model of the robots mechanics/actuators, whereas when operating a physical sensing agent the code is interfaced to the hardware.

Figure 2 shows a 2D representation of the ultrasonic modelling problem, illustrating the air coupled piezoelectric transducers used to generate and receive ultrasonic A_0 Lamb waves. Instead of performing a finite element analysis of the complete system which would be prohibitively computationally expensive, the model is broken into sections. A Linear Systems Model [9] is an unidimensional model of a piezoelectric ultrasonic transducer and can be used to calculate the impulse response function. A Local Interaction Simulation Approach (LISA) [8, 16, 17] is used to model wave propagation in the plate, and a ray tracing approach is adopted to interface between the two models.

Previous Lamb wave modelling work using a LISA approach [18, 19] has simplified the simulation to a 2D problem in the X-Y plane, and modelled a single Lamb wave mode as a bulk wave with the same velocity. This approach however does not simulate different modes and cannot accommodate effects of mode conversion, dispersion and allowance for defects that are not full

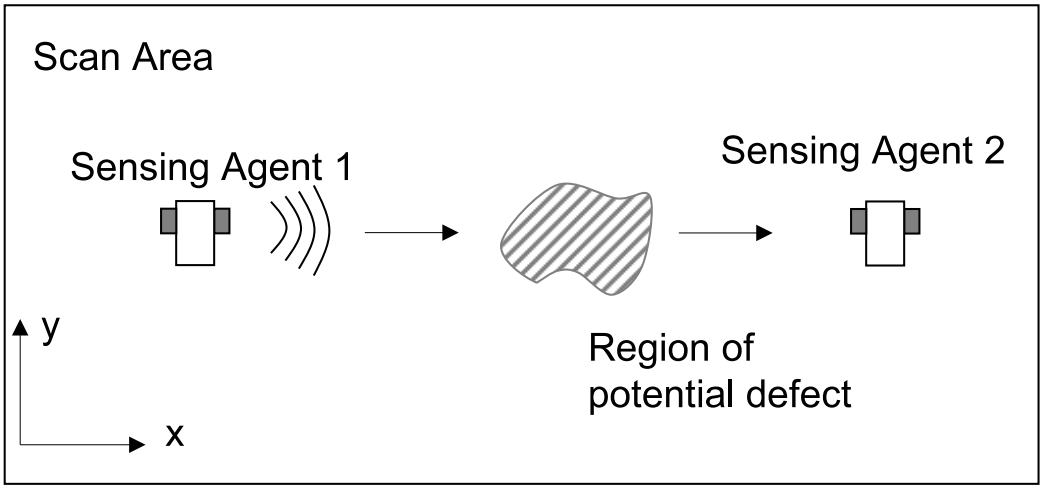

Figure 1: Basic Geometry for the sensing agent scanning. Each sensing agent (1,2) carries an air-coupled ultrasonic transducer which can be used for transmission or reception. Sensing agent positions are independently controlled across the scanned area.

thickness. Additionally since an X-Y model cannot model the out-of-plane displacement it is unsuitable for the current application where the out-of-plane motion of the A_0 mode is fundamental to the measurement process.

To avoid this problem, two scenarios were considered by the authors. Firstly a 2D X-Z plane model (considering a plate of infinite width) was used to validate the LISA model and determine the required mesh resolution. Secondly a complete 3D model using LISA was created which allowed Lamb wave propagation in both the X and Y dimensions to be simulated. Since the 3D simulations were significantly more computationally expensive than their 2D counterparts, they were only performed when the test geometries considered made them essential.

3. Local Interaction Simulation Approach (LISA)

Finite difference and finite element are standard techniques used for wave propagation modelling, examples include [20, 21, 22]. Finite element models are able to cope with complex geometries but do not have the ease of implementation of finite difference based models. In particular, when the sample geometry is relatively simple (e.g. a rectangular plate), then finite difference techniques become increasingly attractive in terms of ease of implementation.

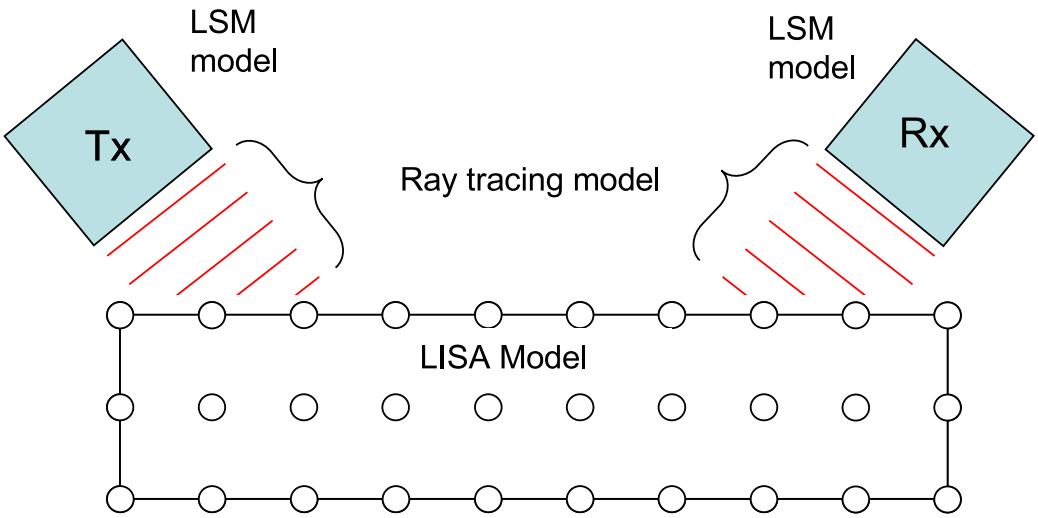

Figure 2: 2D representation of ultrasonic propagation simulation. Tx and Rx are modelled with linear systems approach. Plate is discretised into nodes for either finite element or LISA model.

The LISA technique is similar to finite difference modelling in that it discretises the modelling problem temporally and spatially to a series of iterative equations. With LISA the model is created heuristically from a discretised model, whereas in fintie difference modelling the partial differential equations (PDE) that describe a continuous model are discretised using finite difference formulation [23]. Importantly LISA bypasses the approximation made by finite difference when it converts derivatives into finite differences that leads to severe errors at sharp discontinuities, making LISA more accurate for inhomogeneous simulations. Delsanto et al pioneered LISA development and have shown [16] direct comparison between finite difference modelling, LISA and a analytical solution for wave propagation in a bilayer.

3.1. Theory

The LISA algorithm (Equation 1) is relatively straight-forward in one dimension.

$$w_i{}^{t+1} = Tw_{i-1}{}^{t} + T'w_{i+1}{}^{t} - w_i{}^{t-1} \tag{1}$$

where

$$T = \frac{2}{1+\zeta} \quad T' = \frac{2\zeta}{1+\zeta} \quad \zeta = \frac{Z_1}{Z_2}$$

This iterative equation gives the displacement of a gridpoint w_i at the next timestep $(t+1)$, relative to the displacement of the gridpoint at the previous timestep and the displacement of the gridpoint on each side $(i+1$ and $i-1)$. The transmission coefficients T and T' allow for propagation through a heterogeneous medium (multilayers in the 1D case) with acoustic impedance Z. The algorithm assumes homogenous material properties in each cell, but cells can have different material properties - referred to as the Sharp Interface Model (SIM) [16]. Equation 1 assumes that the nodes are spaced for stability, a condition governed by Equation 2.

$$v\tau/\epsilon <= 1 \tag{2}$$

where v represents the longitudinal velocity of sound in the medium, τ the timestep and ϵ the cell size. The LISA iteration equation can easily be extended to 2D [16] and 3D [17] geometries. Readers are referred to [8] for a full derivation of the 1D algorithm.

An abridged derivation of the 2D algorithm will now be presented, starting with the elastodynamic wave equation [24]:

$$\partial_l(S_{klmn}\partial_n w_m) = \rho\ddot{w}_k \qquad (k,l,m,n = 1,3) \tag{3}$$

where S is the stiffness tensor, ρ is the material density and w is the particle displacement. Ignoring antiplane shear waves to concentrate on two-dimensional wave propagation, this can be simplified to:

$$\partial_k(\sigma_k w_{k,k} + \lambda w_{h,h}) + \partial_h[\mu(w_{k,h} + w_{h,k})] = \rho\ddot{w}_k \tag{4}$$

$$(k = 1,2, h = 3-k = 2,1)$$

where $\sigma_k = S_{kkkk}, \lambda = S_{1122}, \mu = S_{1212}$ and a comma preceding a subscript denotes differentiation with respect to that variable. λ and μ are the Lamé constants for the material.

For a homogenous specimen, Equation (4) can be rewritten as,

$$\sigma_k w_{k,kk} + \mu w_{k,hh} = v w_{h,kh} = \rho\ddot{w}_k \qquad (k = 1,2, h = 2,1) \tag{5}$$

where $\upsilon = \lambda + \mu = \sigma - \mu$. In matrix form this can be written as,

$$AW_{,11} + BW_{,22} + CW_{,12} = \rho\ddot{W} \tag{6}$$

where: $A = \begin{pmatrix} \sigma_1 & 0 \\ 0 & \mu \end{pmatrix}$, $B = \begin{pmatrix} \mu & 0 \\ 0 & \sigma_2 \end{pmatrix}$, $C = \begin{pmatrix} 0 & \upsilon \\ \upsilon & 0 \end{pmatrix}$ and $W = \begin{pmatrix} w_1 \\ w_2 \end{pmatrix}$

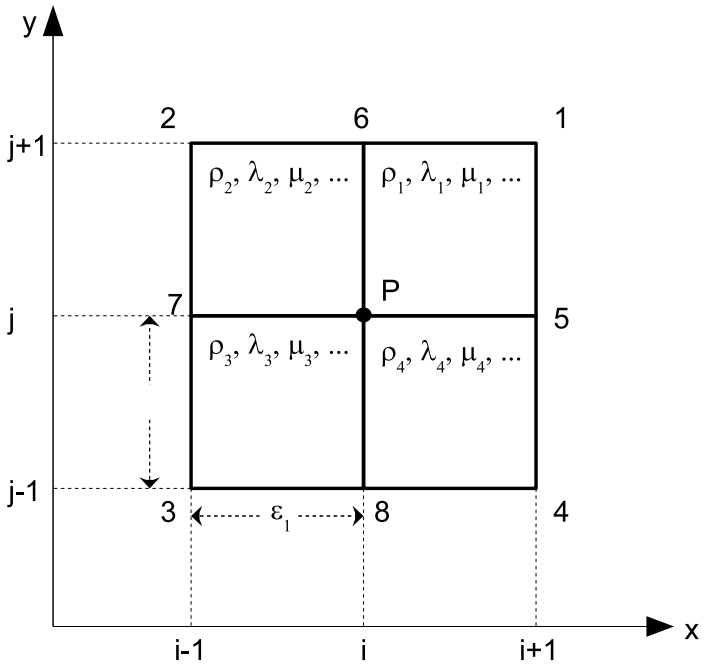

Figure 3: LISA spatial discretisation

In a 2D LISA simulation the structure is discretised into cells, as shown in Figure 3. Each nodal point P is at the junction of four cells. The second time derivatives across the four cells are required to converge towards a common value at the point P, which ensures that if the cell displacements are continuous at P for the two initial times t = 0 and t = 1, they will remain continuous for all later times.

Using a finite difference scheme for the spatial first derivatives in the four surrounding cells to P, gives four equations in eight unknown quantities $\{w_{m,n}\}, m = 1, ..., 4, b = 1, 2$. These equations are omitted here for space reasons. Imposing continuity of the stress tensor τ at the point P and using further finite difference formulae gives four additional equations in the

unknown quantities $\{w_{m,n}\}$, thus allowing these unknown spatial first derivatives to be solved.

The following definitions are made,

$$g_i = \lambda_i - \mu_i \tag{7}$$

${\sigma_c}^{(d)}$ is the stiffness tensor in cell c in direction d, c = 1,4, d = 1,2.

$$\sigma^{(d)} = \frac{{\sigma_1}^{(d)} + {\sigma_2}^{(d)} + {\sigma_3}^{(d)} + {\sigma_4}^{(d)}}{4} \tag{8}$$

$$\mu = \frac{\mu_1 + \mu_2 + \mu_3 + \mu_4}{4} \tag{9}$$

$$\rho = \frac{\rho_1 + \rho_2 + \rho_3 + \rho_4}{4} \tag{10}$$

$$\sigma^5 = \frac{\sigma_1 + \sigma_4}{2}, \sigma^6 = \frac{\sigma_1 + \sigma_2}{2}, \sigma^7 = \frac{\sigma_2 + \sigma_3}{2}, \sigma^8 = \frac{\sigma_3 + \sigma_4}{2} \tag{11}$$

The particle displacements in the x and y directions in Figure 3 are denoted as u and v respectively. Recalling that $\upsilon_i = \lambda_i + \mu_i$, after a certain amount of algebra, these u and v displacements at the point P can be calculated as,

$$\begin{aligned} u_{t+1} = & \\ & 2u_t - u_{t-1} + \frac{1}{\rho}[{\sigma_5}^{(1)}u_5 + {\sigma_7}^{(1)}u_7 + \mu_6 u_6 + \mu_8 u_8 \\ & - 2(\sigma^{(1)} + \mu)u_t - \frac{1}{4}\sum_{k=1}^{4}(-1)^k \upsilon_k v_t \\ & - \frac{1}{4}\sum_{k=1}^{4}(-1)^k \upsilon_k v_k + \acute{g}_5 v_5 + \acute{g}_6 v_6 + \acute{g} v_7 + \acute{g}_8 v_8] \end{aligned} \tag{12}$$

$$\begin{aligned} v_{t+1} = & \\ & 2v_t - v_{t-1} + \frac{1}{\rho}[\mu_5 v_5 + \mu_7 v_7 + {\sigma_6}^{(2)}v_6 + {\sigma_8}^{(2)}v_8 \\ & - 2(\sigma^{(2)} + \mu)v_t - \frac{1}{4}\sum_{k=1}^{4}(-1)^k \upsilon_k u_t \\ & - \frac{1}{4}\sum_{k=1}^{4}(-1)^k \upsilon_k u_k + \acute{g}_5 u_5 + \acute{g}_6 u_6 + \acute{g} u_7 + \acute{g}_8 u_8] \end{aligned} \tag{13}$$

where: $\acute{g}_5 = \frac{1}{2}(g_4 - g_1)$, $\acute{g}_6 = \frac{1}{2}(g_1 - g_2)$, $\acute{g}_7 = \frac{1}{2}(g_2 - g_3)$ and $\acute{g}_8 = \frac{1}{2}(g_3 - g_4)$ Equations 12 and 13 are the principal displacement equations of LISA in two dimensions. A more detailed derivation can be found in [16], although note that a number of small errors present in the formulae within that paper have been corrected in [18] and [19]. These two equations rely solely on known material properties σ, λ and μ for each cell and arbitrary discretisation steps, both spatial and temporal.

A simulation of wave propagation in an aluminium plate may consist of a layer of cells surrounded by a thin layer of air. The material properties can be defined for each cell, so defects such as slots can be easily represented by replacing some of the plate cells with air cells. The fundamental simplicity of the LISA algorithm allows for highly efficient implementation and since the LISA discretisation is regular, the locations of cells do not need to be stored in memory, but can be calculated at run time further improving speed while reducing memory requirements. Since each node has to be individually calculated, LISA does not scale particularly well - as volume increases linearly, the number of nodes increases by a factor of three. However this is a general problem with discritisation in finite difference and finite element models and not specific to LISA. Importantly, since each node only depends on its nearest neighbours, the model lends itself well to parallelisation. This opens the way for future work to potentially implement the LISA modelling task itself across a fleet of sensing agent vehicles each with its own microcontroller based acquisition and control system.

4. LISA Validation

In order to validate the LISA propagation model, a comparison between LISA, standard finite element modelling modelling software and numerical solution to the Rayleigh-Lamb frequency equations was performed. Guided waves were chosen for the validation exercise as the presence of multiple modes of propagation, combined with the variation of phase velocity with Frequency Thickness Product (FTP), provided an exacting test of the accuracy of the results.

4.1. Dispersion

An approach [25] based on a spatially sampled impulse response function, followed by a 2D FFT was used to recover the spatial and temporal frequency components of the propagating waves. A 2D simulation of a 250mm long,

infinitely wide, 1mm thick aluminium plate was preformed. The plate was excited with a single cycle of a sine wave ($2\mu s$ duration with 0.125mm spatial diameter) and spatially sampled to create a series of discrete time surface displacement measurements as shown in Figure 4. The excitation was applied to a distance of 1/3 into the plate (83mm) and the simulation was run only until the wave reached the outer edge of the plate to ensure no edge reflections were present. Taking a 2D FFT of this time-space data matrix produced a frequency-wavenumber [f-k] space data which was plotted to reveal the dispersion of the propagating waves; as shown in Figure 5.

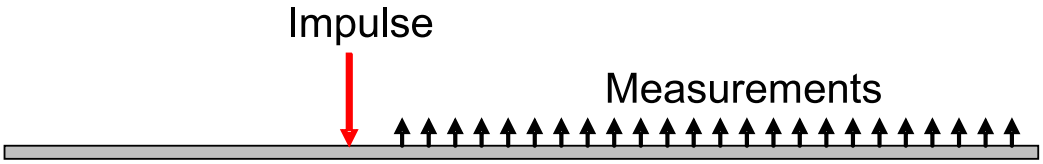

Figure 4: Simulation of spatially sampled broadband wave propagation in a plate

Figure 5 shows a contour plot of the [f-k] dispersion matrix, which exhibits good agreement with analytic theory [26] shown as dashed lines. The multiple modes are clearly visible and of the correct shape. This plot was generated using a 2D LISA model where the 1mm thickness was divided into 8 cells. To compare the accuracy of fit of the simulation with the numerical solutions of 'Disperse' [26], a method of extracting the local maxima of the dispersion curves was developed, followed by calculation of an error function. A filter was written to automatically extract the local maxima in the [f-k]dispersion plot. The filter considered each pixel in the image and subtracted the mean of the surrounding N^2 pixels (N = 14 was found to work best). It then normalised the data and set any point with a value below 50% to 0 and anything above 50% to 1. Finally the filter replaced any small clusters of points with a single point equal to the average.

Figure 6 shows the filter applied to the data of Figure 5 to extract the local maxima.

In order to have an objective measure of the goodness of fit, the normalised mean-square error (MSE) is introduced, the definition is:

$$MSE(\hat{x}) = \frac{100}{N\sigma_x^2}\sum_{i=1}^{N}(x_i - \hat{x}_i)^2 \tag{14}$$

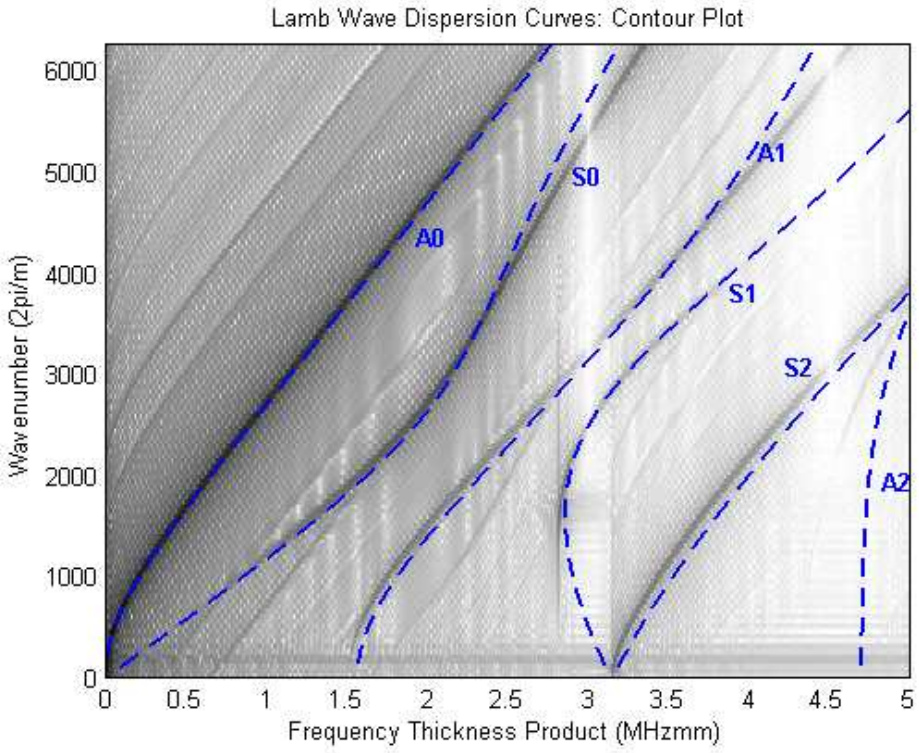

Figure 5: Contour plot of Lamb wave dispersion matrix: LISA simulation results for 2D model, plate thickness 1mm, 8 cells

where the caret denotes an estimated quantity. This MSE has the following useful property; if the mean of the output signal $\overline{x}$ is used as the model i.e. $\hat{x}_i = \overline{x}$ for all i, the MSE is 100.0, i.e.

$$MSE(\hat{x}) = \frac{100}{N\sigma_x^2}\sum_{i=1}^{N}(x_i - \overline{x})^2 = \frac{100}{\sigma_x^2}.\sigma_x^2 = 100$$

Experience shows that a MSE of less than 5.0 indicates good agreement while one of less than 1.0 reflects an excellent fit.

The accuracy of LISA was measured by calculating the normalised mean squared error of dispersion curves using 'ideal' data generated numerically by Disperse [26]. $\hat{x}_i$ is the frequency thickenss product of a sample from the LISA dispersion plot and x_i is the corresponding point from Disperse for the

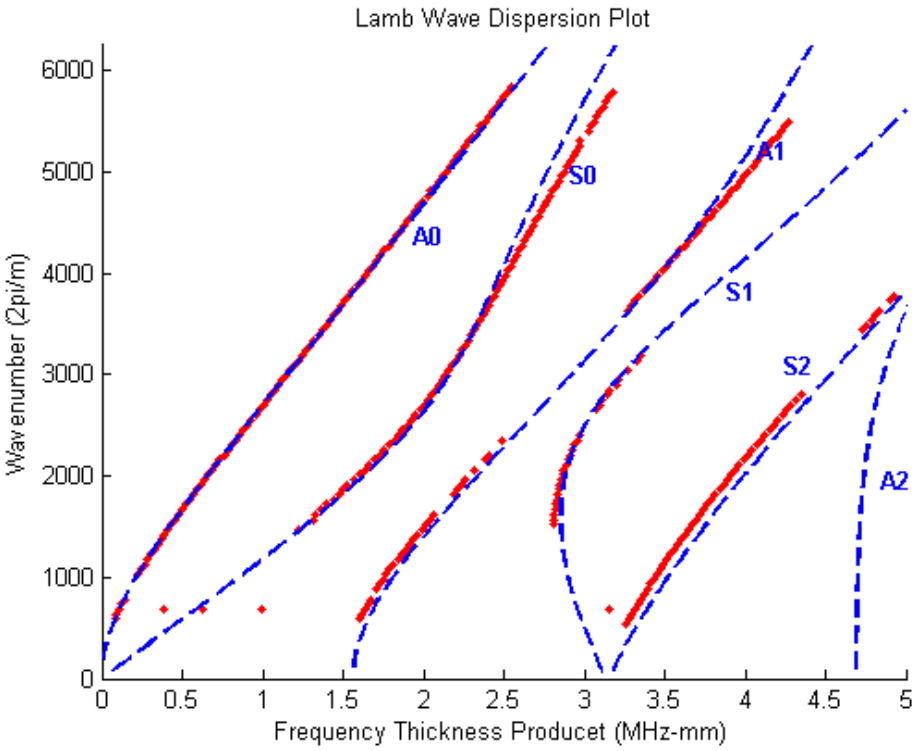

Figure 6: Comparison between automatic local maxima extraction algorithm and numerical solution (dashed lines)

same wavenumber (using linear interpolation between discrete data points where required).

4.2. Cell density considerations

One of the most significant parameters in the implementation of LISA is the mesh density. Increasing the density improves the accuracy, but increases the computational complexity of the model. In 2D simulations, fine meshes do not present such a problem, as most simulations take less than a few minutes to run. However in 3D, the computation is more involved and run times can reach several hours. It should be noted that to maintain stability, halving the cells size also requires the time step to be halved, as indicated in Equation 2. In 3D, halving the time step increases the run time by a power of four (double the number of cells in each dimension plus double the total number of frames). Memory requirements scale linearly with the number of

cells, making large 3D simulations prohibitive on desktop workstations. Mesh Sensitivity Analysis showed that reducing the cell size (hence increasing the density) improved the correlation with theory. The results are shown in Figure 8.

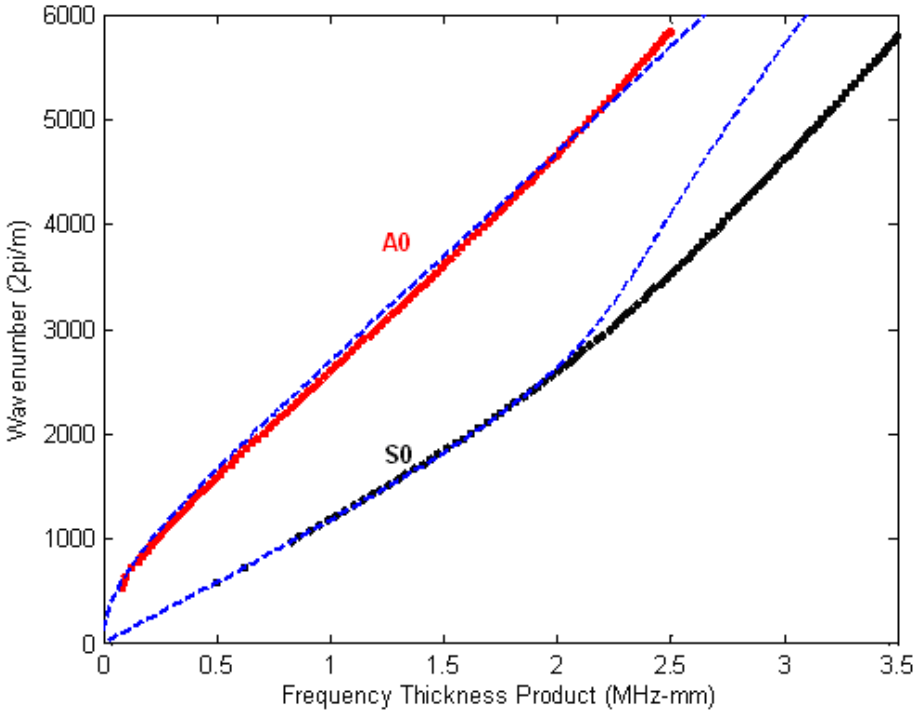

Figure 7: LISA simulation of 1mm thick plate with 4 cells through the thickness - showing the S_0, A_0 modes and analytic solution (dashed lines)

It should be noted that since the current sensing agent platforms selectively generate and receive just the A_0 mode, good correlation with A_0 is likely to be sufficient for current applications. The minimal functional density is 2 $cells/mm$, which gives a reasonable approximation of A_0 with a MSE of 1.6, however no other modes are present. Increasing to 4 cells/mm provides an excellent approximation of A_0 (MSE = 0.13) and a reasonable approximation of S_0 (MSE =4.3), this is shown in Figure 7, noting that S_0 diverges from the analytical solution for FTP $>$ 2 MHzmm. In order to get an excellent match for both A_0 and S_0 (MSE $<$ 1) the cell density must be

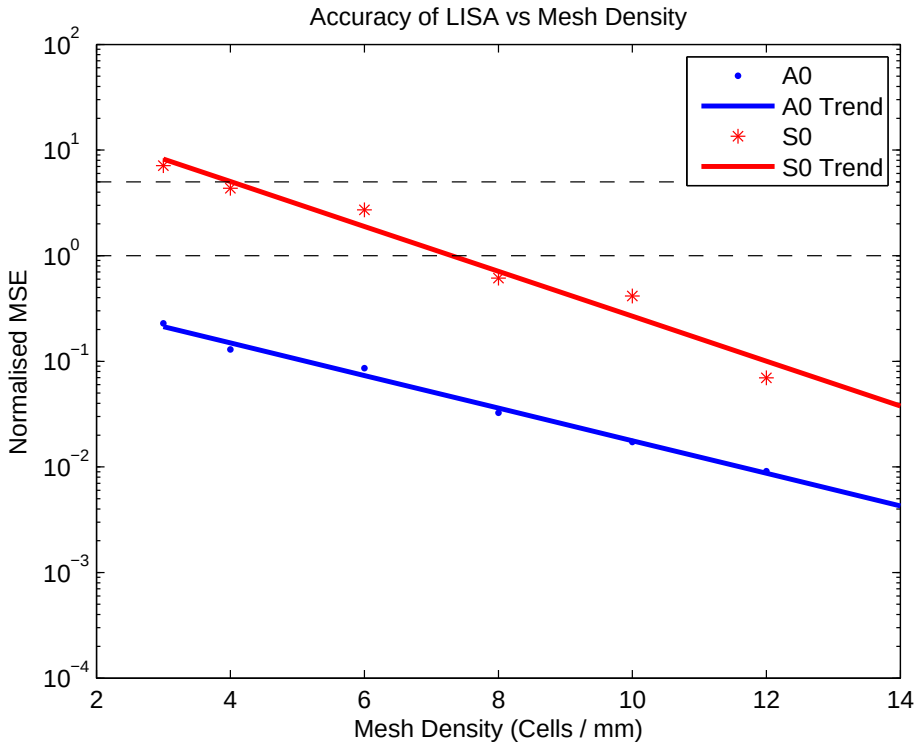

Figure 8: Variation of LISA accuracy(2D) as a function of mesh density expressed as MSE from analytic model. The horizontal dashed lines represent MSE = 5 - good agreement and MSE = 1 - excellent agreement

increased to 8 cells/mm. This is shown in Figure 5 which also shows the higher order modes.

5. Comparison with a Commercially Available Package

The low level control provided by custom implementation facilitates interfacing with other models, such as the linear systems model, that would not be straightforward with a commercial closed-source package. However, in order to fully justify the use of LISA over commercial finite element packages, a comparison was performed between LISA and a leading simulation package PZFlex [7] to compare accuracy and calculation speed.

5.1. Accuracy

As discussed in Section 2 a 3D simulation is required for high accuracy. However as discussed in section 4.2 the computational intensity of 3D models often results in prohibitively long run times and hardware requirements making a coarser mesh with a reduction in accuracy a practical choice. As expected PzFlex followed the same trend. The publishers of PzFlex recommend a minimum of 20 cells throughout the thickness for a Lamb wave plate simulation, however this is impractical in 3D, so a mesh sensitivity study was performed in 2D to determine how the accuracy degraded with the cell density. The results for PzFlex are shown in Figure 9. It was found that below 6 cells/mm PzFlex did not produce coherent results and that 6 cell/mm provided a good match for A0 and a reasonable match for S0 (MSE = 0.16 and 3.3 respectively) - Figure 10 which should be compared with the 4 cells/mm result for LISA shown in Figure 7.

5.2. Speed

Using LISA with 4 cells/mm through the thickness provided a good tradeoff between speed and accuracy and was roughly equivalent to 6 cells/mm for PzFlex. Both provide a good approximation of A_0 and a reasonable approximation of S_0 which diverges at higher wavenumbers, as shown in Figures 7 and 10.

In order to compare the simulation speeds a 250x250x1mm aluminium plate was modelled in 3D using 4 cells/mm for LISA and 6 cells/mm for PzFlex. The simulation was identical to that preformed in Section 4.1 except the 3D geometry was modelled. The simulations were set to run for $90us$ of simulation time. The results are shown in table 5.2. The comparison was performed on a Windows XP (64 bit edition) 2.4GHz quad-core workstation (2 dual AMD Opterons) with 16GB RAM.

Table 1: PZFlex vs LISA speed comparison

Package	Time to run 90us simulation
PzFlex	2 hours 58 minutes
LISA	53 minutes

It is clear that in this instance the custom LISA propagation code outperformed the commercial package by a factor of approximately 3.

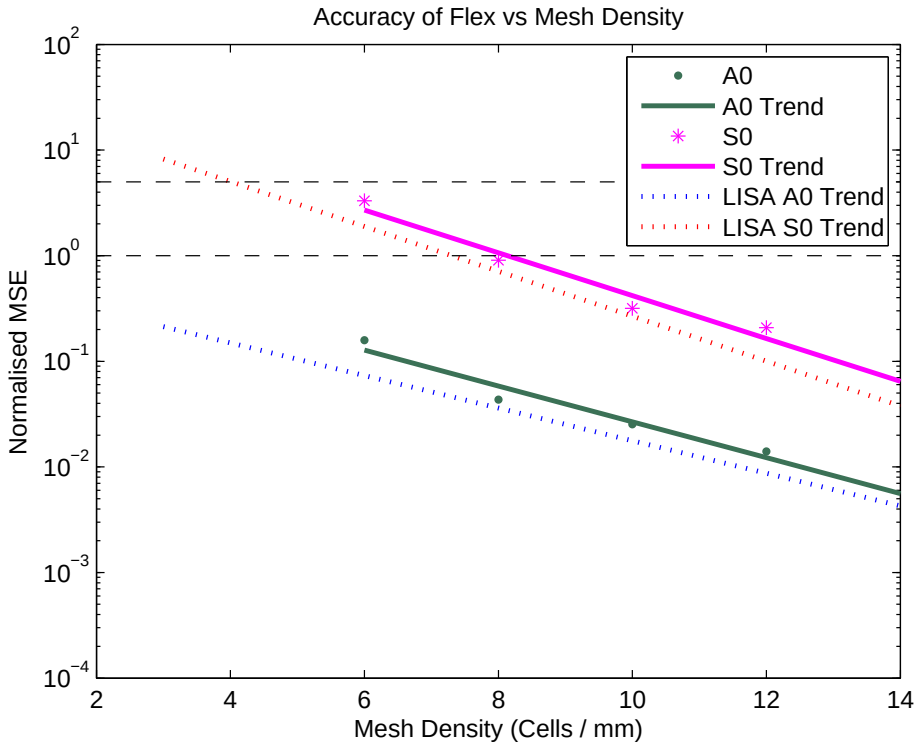

Figure 9: Accuracy comparison (2D) between LISA and PzFlex as function of mesh density. The horizontal dashed lines represent MSE = 5 - good agreement and MSE = 1 - excellent agreement

6. Angled Transducers

This section links the linear systems model with the LISA wave propagation model to create an angled transducer pitch-catch model, to simulate air-coupled Lamb wave generation and detection, as required by the sensing agents.

6.1. Linear Systems Model

A Linear Systems Model [9] was used to model response of the transmitter and receiver transducers. The input drive or received signal was convolved with the simulated transducer impulse response. This work has previously been published by some of the authors [27], [11] so will not be discussed in detail. 1-3 piezocomposite transducers were designed to operate at a centre

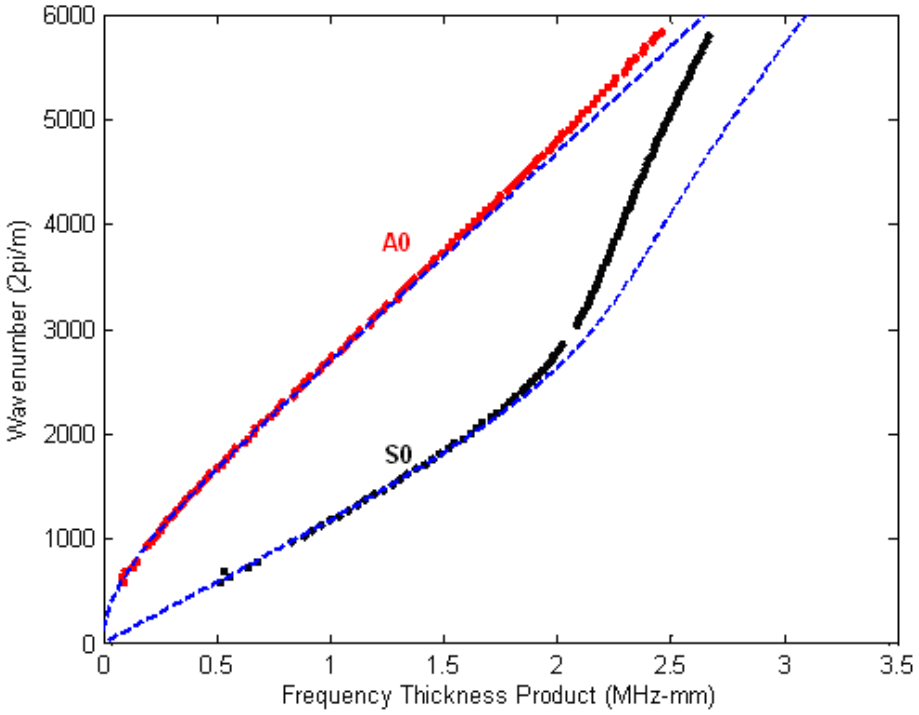

Figure 10: PzFlex simulation of 1mm thick plate with 6 cells though the thickness - showing A_0, S_0 modes and analytic solution (dashed line)

frequency of 600kHz in pitch-catch mode. The transmitter had a 70% volume fraction of PZT-5H and the receiver had a 30% volume fraction of PZT-5A. In both cases the passive filler material was epoxy (CY1301/HY1300). A special low-loss matching layer was integrated onto the front-face of each transducer to minimise insertion loss due to the impedance mismatch between the transducer face and air. This transducer assembly is modelled and evaluated in [10].

6.2. A_0 Lamb Wave Generation

When the transmitter is excited the axial mode produces a planar wave radiating from the front face (as shown in Figure 11). Efficient matching ensures most of the energy radiates from the front of the transducer [10]. Also, if a 1-3 piezocomposite is used, the composite nature of the transducer helps to damp out unwanted radial modes. The angle θ was selected to phase

match the transducer output to the desired Lamb wave mode as described by Snell's Law. For propagation in a 1mm thick aluminium plate at 600 kHz the appropriate value of θ i =9.5 degrees (c_{ph} = 2060 m/s).

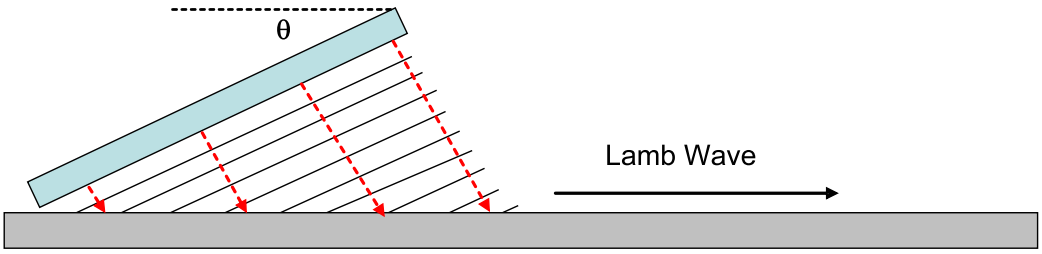

Figure 11: Air-coupled generation of A_0 Lamb mode in aluminium sample plate

A ray tracing technique was used to model the excitation of the specimen under test. For each LISA node under the transmitter, an excitation was applied at an angle perpendicular to the transmitter. The air channel was modelled as a delay (assuming no attenuation). Nodes near the base of the transducer were excited first, with the delay increasing with distance from the base. Note it could take several cycles before the whole area under the transducer was excited. Incorporating a model of the near field [28] fell outwith the scope of this work, but the loss in accuracy is minimal since slight variations in the amplitude across the excitation wave are averaged over the Lamb wave as it passes through the excitation region. Since the transducer beam interferes with the plate well inside the near field beam spread in negligible.

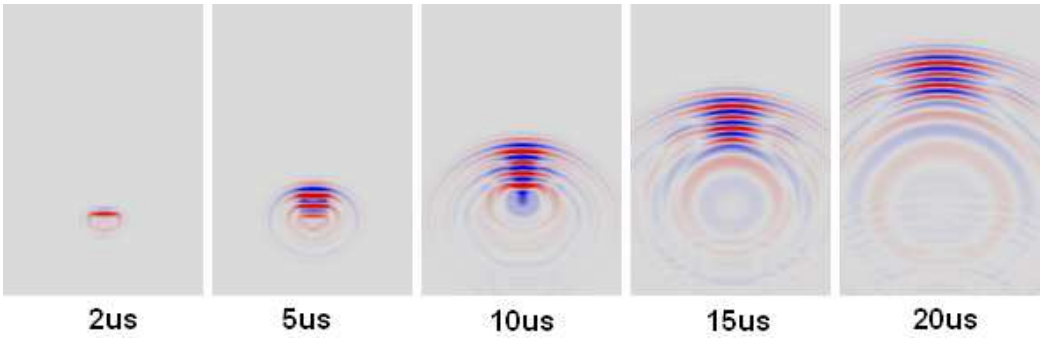

Figure 12: Simulation of air-coupled A_0 generation in a 1mm thick aluminium plate

Figure 12 shows an example simulation of a 10mm circular transducer

placed over a 1mm aluminium plate, the Figure illustrates the amplitude of the out-of-plane displacement. The transducer was excited with a 600kHz, 3 cycle tone burst and was set at an angle of 9.5^o facing forward (angle in XY plane = 0^o). The A_0 wavepacket can be clearly seen.

6.3. A_0 Lamb Wave Measurement

Snell's law works reciprocally, so for matched reception, the angle of the receiver must be the same as that of the transmitter, allowing the wave to recombine constructively on the receiver's face. Again a ray tracing approach was adopted, where only nodes that fell under the transducers field of view were considered. For each node the component of displacement normal to the receiver face was added to the receiver with a time delay corresponding to the perpendicular distance between the node and transducer face. At each time-step the transducer model integrated over all inputs to produce a single output.

7. Interfacing the Linear Systems Model and LISA

The LISA model simulates the displacement field generated by elastic wave propagation in the sample under investigation, whereas the linear systems model approximates the pressure field output from a transmitter excited by a voltage, or the voltage generated by the incident wave on the receiver's face. In order to interface the two models the excitation pressure wave must be converted to a displacement excitation for LISA and the resulting displacement wave under the receiver must be converted back to a pressure wave. Equation 15 can be used to perform this conversion, where Z is the acoustic impedance of the plate and v_{node} is the velocity of the point in question.

$$P = Zv_{node} \tag{15}$$

v_{node} can be calculated by differentiating the displacement w.

$$P_t = Z(\frac{w_t - w_{t-1}}{\tau}) \tag{16}$$

The last thing that has to be considered is the impedance mismatch between the plate and surrounding air. The transmission coefficient can be estimated from Equation 17.

$$T_P = \frac{P_t}{P_i} = \frac{2Z_2}{Z_1 + Z_2} \tag{17}$$

P_t and P_i are the transmitted and incident pressure waves respectively travelling into a material with acoustic impedance Z_2 from a material with acoustic impedance Z_1 at normal incidence. The excitation pressure used to calculate the excitation displacement in equation 15 is calculated by multiplying the output from the transmitter model by the transmission coefficient for air to aluminium. The pressure used as the input to the receiver model is first calculated by equation 15 then multiplied by the transmission coefficient for aluminium to air.

7.1. Simulation Results

Figure 13 shows a full simulation of a time domain pitch-catch experiment between angled transducers, incorporating both LISA and the Linear Systems Transducer model compared with experimental measurements. The excitation was a 3 cycle tone burst of 10V at 600kHz and the separation between the transducers was 100mm. The transducers were the same as those described in Section 6.1 and had an active area of 30mm x 30mm. The transmitter was driven directly from the 50Ω output of an Agilent 33220A function generator. The receiver was amplified by 40dB using a Olympus 5670 preamplifier and connected to the 1MΩ input of an Agilent 54624A oscilloscope.

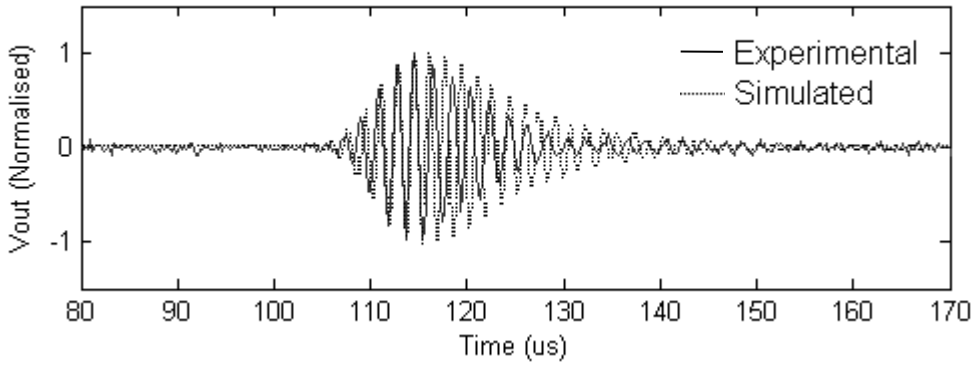

Figure 13: Time domain comparison between simulated response (dashed line) and experimentally measured response (solid line) of air-coupled A_0 generation, propagation and reception in 1mm thick aluminium plate

Figure 14 shows five 3D pitch-catch simulations between 10mm diameter angled transmitter and receivers. For clarity the diagrams are drawn in 2D.

The plate was 125mm x 125mm x 1mm. The transmitter was positioned at x = 62.5mm, y = 25mm at an angle of 9.8 degrees to the surface. In case I a point probe was placed to measure the out-of-plane displacement on the top surface at x = 62.5mm, y = 100mm. In case II an angled receiver was placed in the same location as the probe positioned to face the transmitter and held at 9.8 degrees (XZ). In case III, the receiver was rotated about to face away from the transmitter. Case IV and V are the same as case II, with the addition of void regions in the model to simulate defects. In Case IV the defect is a 0.5 mm deep surface breaking void which is 3mm long in the Y direction, it is 10mm wide in the X direction and positioned 80mm in from the plate edge 'C' (62.5mm, 80mm and 0.75mm in X, Y and Z respectively). In Case V the defect is extended to be 10mm long in the Y direction and is positioned in the centre of the plate thickness (62.5mm, 80mm and 0.5mm in X, Y and Z respectively).

Figure 15 shows the normalised output for each case (in cases III - IV, the amplitudes are normalised against case II). In case I, four wave packets are visible which represent the initial wave passing under the probe (A-B), the reflection from the back edge (A-C-B), the reflection from the back edge reflected off the front edge beside the transducer (A-C-D-B) and finally the packet reflected again off the back edge (A-C-D-C-B). The probe is assumed to be ideal so only the transmitters transfer function is included. In cases II - V a narrow band piezocomposite receiver is used which causes the signals to take longer to decay. In case II only the first and third packets are visible since the receiver is only sensitive to incident waves. This directional sensitivity is also apparent in case III where only the back wall reflections are visible. In cases IV and V the effect of the defect can be clearly seen, the direct packet is heavily attenuated, there is also a slight delay in the peak caused by some of the energy travelling around the defect. It should be noted that the system is sensitive to voids that are not 100% through the thickness which may be obscured in visual inspection.

Figure 16 shows a simulated scan of a 250mm $\times$ 250mm 1mm thick aluminium defect with two artificial defects. The transducers had a 10mm diameter and were driven at 600kHz. The defects were 100% through the plate width and were located at (90mm, 170mm) and (150mm ,115mm) with dimensions of 10mm $\times$ 10mm and 10mm $\times$ 2mm respectively. The second defect was rotated by 30^o relative to the x axis. A single sensing agent

scanned in pulse-echo configuration from (30mm, 30mm) to (220mm, 30mm) in 5mm intervals. This required 39 individual simulations which could be run in parallel over several computers as there was no need for the simulations to be run sequentially. The results are shown as a 2D grayscale plot of the envelope detected receiver time traces. The 'Y' axis was converted from time to distance using the group velocity of the A_0 mode in 1mm aluminium. The result of the scan is shown in Figure 17, the image was interpolated linearly by a factor of 5 in the 'X' direction to improve the quality of the image. The 10mm $\times$ 10mm defect is clearly visible whereas the 10 $\times$ 2mm defect has reduced visibility due to the incident Lamb wave being reflected away from the transducer. The back wall is clearly visible with two shadows caused by the defects.

8. Conclusions

A full simulation for an air-coupled ultrasonic scanner for deployment on mobile robotic platforms has been presented and validated against experimental measurements. Generation and reception of ultrasonic Lamb waves was accomplished using air-coupled piezocomposite transducers whose response was modelled using a previously described [9] Linear Systems Model. Propagation in sample plates was simulated using a the LISA model. This was used instead of conventional finite element modelling for two reasons. Firstly to be useful for modelling adaptive inspection strategies implemented by the sensing agents the execution speed of the code is critical. For complex geometries, high calculation times would make it unfeasible for optimisation over different propagation paths to be considered. Secondly the LISA code could be combined with both the linear systems model of the transducer Tx/Rx response and the ray tracing approach adopted to couple between the linear systems model and LISA. The LISA propagation model was extensively validated by comparison of Lamb wave propagation to both a commercial simulation package and a numerical solution to the Rayleigh/Lamb frequency equations.

The complete model was coded in C++ and could be run interactively using a custom GUI running in Windows or in batch mode in either Windows or Linux. The batch code could be configured to run on a High Performance Computer (HPC) allowing multiple simulations to be run in parallel on separate nodes. This is particularly effective for parameter sweeps and for tomographic imaging which requires a series of projections and was used

to create Figure 17. Since the code is cross platform it can be compiled to run on the sensing agent's embedded Linux computer and although limited by onboard memory, simple simulations can be run. Future work will look at distributing the simulation over several sensing agents or alternatively to implement a system where the sensing agent can request a simulation over WiFi which is routed over the internet to a computer offsite that actually runs the simulation. Running the simulation on the sensing agent reduces power required for communications, but increases power required for onboard computation leading to an optimum depending on the simulation complexity.

Future work will consider optimisation of robot scanning strategies for tomographic imaging as possible implementation of LISA for real-time adaptive modification of inspection strategies distributed across the fleet.

Acknowledgment

The authors would like to thank Daley Chetwynd for work rederiving the LISA algorithms in 2D. This research received funding from the Engineering and Physical Sciences Research Council (EPSRC) and forms part of the core research programme within the UK Research Centre for NDE (RCNDE).

References

[1] G. Dobie, W. Galbraith, M. Friedrich, S. Pierce, G. Hayward, Robotic Based Reconfigurable Lamb Wave Scanner for Non-Destructive Evaluation, Ultrasonics Symposium, 2007. IEEE (2007) 1213–1216.

[2] M. Friedrich, Design of miniature mobile robots for non-destructive evaluation, Ph.D. thesis, University of Strathclyde (2007).

[3] R. Farlow, G. Hayward, Real-time ultrasonic techniques suitable for implementing non-contact NDT systems employing piezoceramic composite transducers, Insight 36 (12) (1994) 926–935.

[4] D. Alleyne, P. Cawley, Optimization of Lamb Wave Inspection Techniques.

[5] ANSYS Inc, ANSYS, www.ansys.com (Accessed Dec 2008).

[6] The COMSOL Group, COMSOL, www.comsol.com (Accessed Dec 2008).

[7] Weildlinger Associates, Inc, PxFlex, www.pzflex.com (Accessed Dec 2008).

[8] P. Delsanto, T. Whitcombe, H. Chaskelis, R. Mignogna, Connection machine simulation of ultrasonic wave propagation in materials. I: The one-dimensional case, Wave motion 16 (1) (1992) 65–80.

[9] G. Hayward, J. Hossack, Unidimensional modeling of 1-3 composite transducers, The Journal of the Acoustical Society of America 88 (1990) 599.

[10] G. H. Stephen P. Kelly, T. E. G. Alvarez-Arenas, Characterization and assessment of an integrated matching layer for air-coupled ultrasonic applications, IEEE transactions on ultrasonics, ferroelectrics, and frequency control 51 (2004) no. 10.

[11] A. Gachagan, G. Hayward, S. Kelly, W. Galbraith, Characterization of air-coupled transducers, Ultrasonics, Ferroelectrics and Frequency Control, IEEE Transactions on 43 (4) (1996) 678–689.

[12] F. Mondada, G. Pettinaro, A. Guignard, I. Kwee, D. Floreano, J. Deneubourg, S. Nolfi, L. Gambardella, M. Dorigo, Swarm-Bot: A New Distributed Robotic Concept, Autonomous Robots 17 (2) (2004) 193–221.

[13] B. DAndrea-Novel, G. Bastin, G. Campion, Modeling and Control of Non Holonomic Wheeled Mobile Robots, Proc. of the 1991 IEEE International Conference on Robotics and Automation 1130 (1991) 1135.

[14] Y. Zhao, S. BeMent, Kinematics, dynamics and control of wheeled mobile robots, Robotics and Automation, 1992. Proceedings., 1992 IEEE International Conference on (1992) 91–96.

[15] X. Yun, Y. Yamamoto, Internal dynamics of a wheeled mobile robot, Intelligent Robots and Systems' 93, IROS'93. Proceedings of the 1993 IEEE/RSJ International Conference on 2.

[16] P. Delsanto, T. Whitcombe, H. Chaskelis, R. Mignogna, R. Kline, Connection machine simulation of ultrasonic wave propagation in materials. II the two-dimensional case,", Wave Motion 20 (1994) 295–314.

[17] P. Delsanto, R. Schechter, R. Mignogna, Connection machine simulation of ultrasonic wave propagation in materials III: The three-dimensional case, Wave Motion 26 (4) (1997) 329–339.

[18] B. Lee, W. Staszewski, Modelling of Lamb waves for damage detection in metallic structures: Part I. Wave propagation, Smart Materials and Structures 12 (5) (2003) 804–814.

[19] B. Lee, W. Staszewski, Modelling of Lamb waves for damage detection in metallic structures: Part II. Wave interactions with damage, Smart Materials and Structures 12 (5) (2003) 815–824.

[20] F. Moser, L. Jacobs, J. Qu, Modeling elastic wave propagation in waveguides with the finite element method, NDT and E International 32 (4) (1999) 225–34.

[21] E. Moulin, J. Assaad, C. Delebarre, D. Osmont, Modeling of Lamb waves generated by integrated transducers in composite plates using a coupled finite element–normal modes expansion method, The Journal of the Acoustical Society of America 107 (2000) 87.

[22] D. Alleyne, P. Cawley, The interaction of Lamb waves with defects, Ultrasonics, Ferroelectrics and Frequency Control, IEEE Transactions on 39 (3) (1992) 381–397.

[23] J. Strikwerda, Finite Difference Schemes and Partial Differential Equations, Society for Industrial Mathematics, 2004.

[24] E. S. A.C. Eringen, Elastodynamics, Vol. 1, Academic Press, New York, 1974.

[25] D. Alleyne, P. Cawley, A 2-dimensional Fourier transform method for the quantitativemeasurement of Lamb modes, Ultrasonics Symposium, 1990. Proceedings., IEEE 1990 (1990) 1143–1146.

[26] M. L. B. Pavlakoviec, Disperse: User's manual, Imperial College, Non-Destructive Testing Laboratory.

[27] R. F. Stephen P Kelly, G. Hayward, Applications of through-air ultrasound for rapid NDE scanning inthe aerospace industry, Ultrasonics, Ferroelectrics and Frequency Control, IEEE Transactions on 43 (4) (1996) 581–591.

[28] G. Benny, G. Hayward, R. Chapman, Beam profile measurements and simulations for ultrasonic transducers operating in air, The Journal of the Acoustical Society of America 107 (2000) 2089.

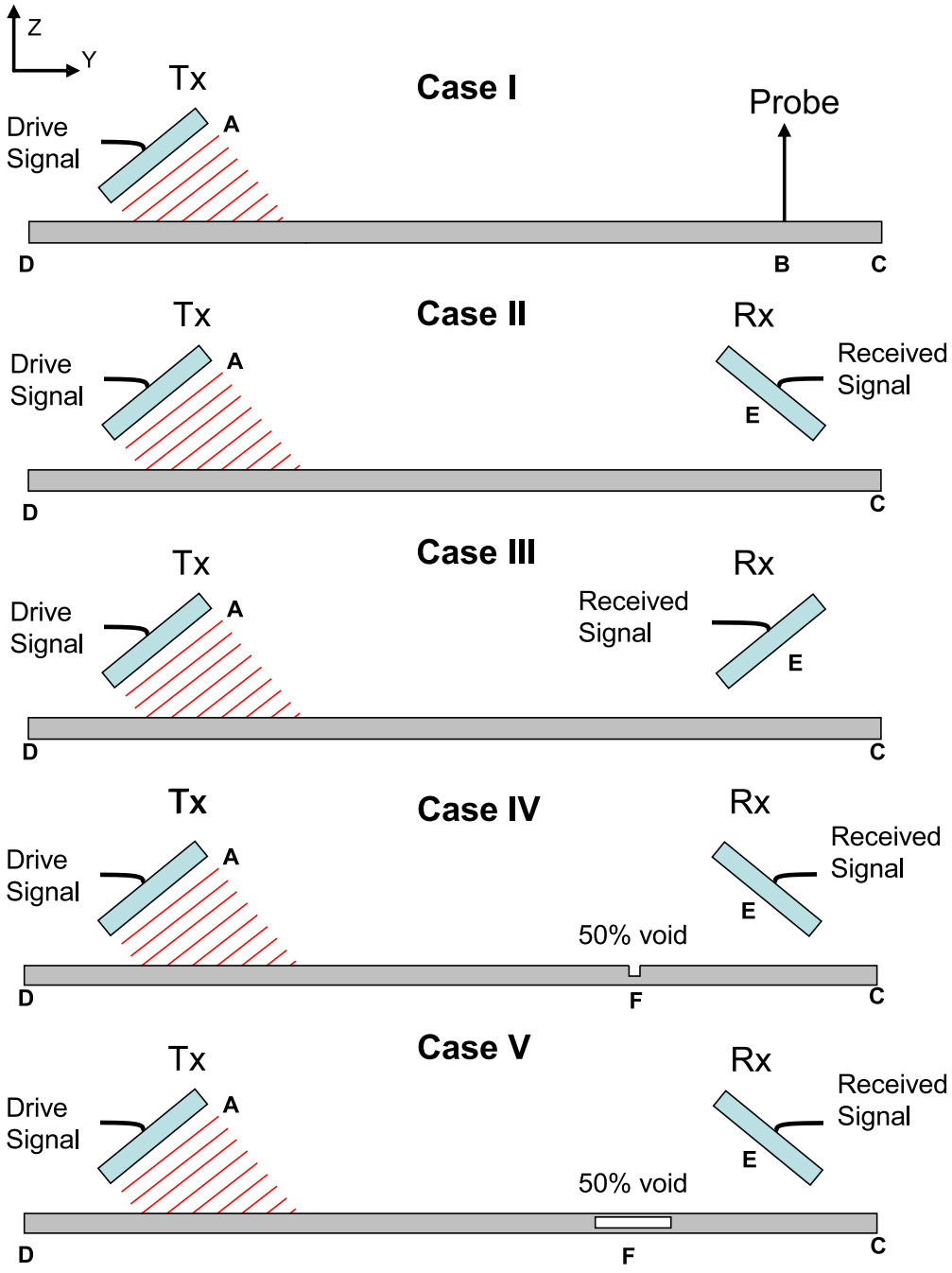

Figure 14: Simulation of pitch-catch ray tracing model combined with LISA

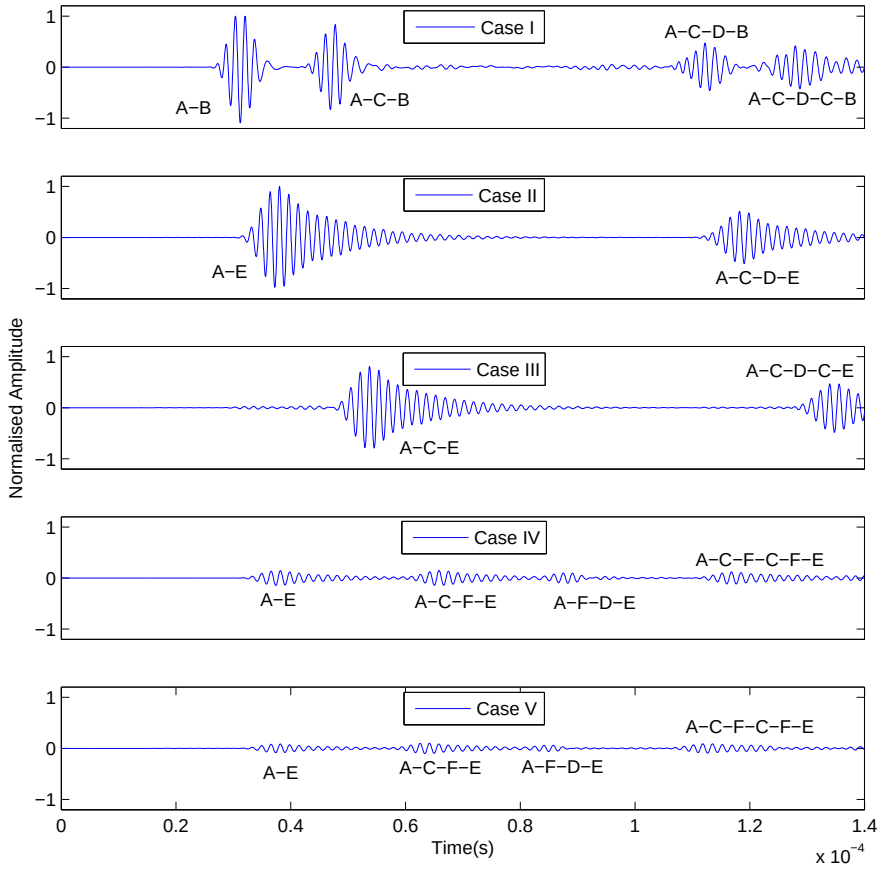

Figure 15: Simulation of pitch-catch geometry combing ray tracing and LISA

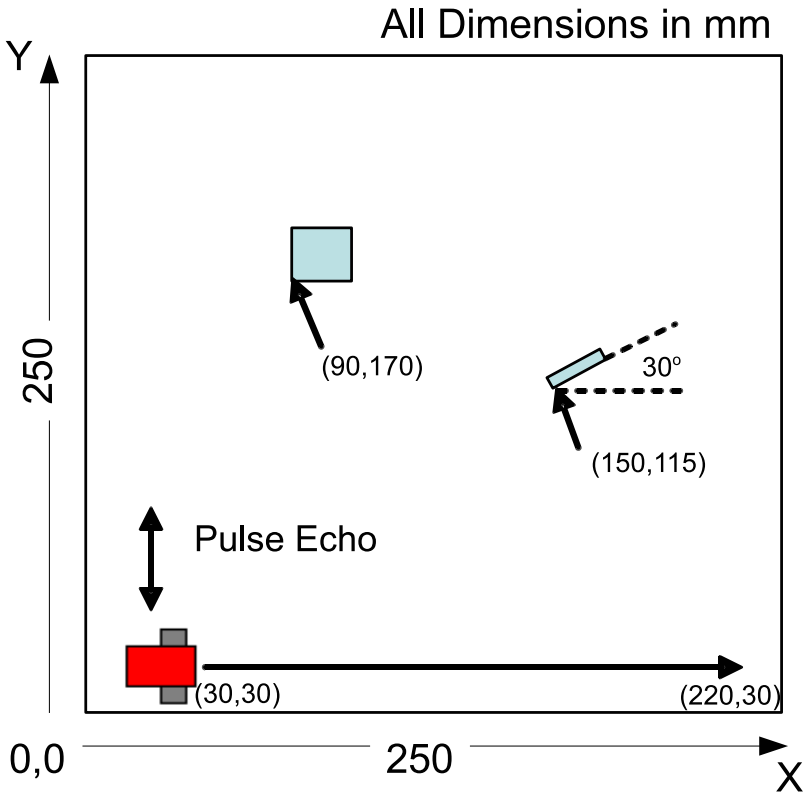

Figure 16: Simulation setup of a 3D pulse-echo inspection using a single remote sensing agent

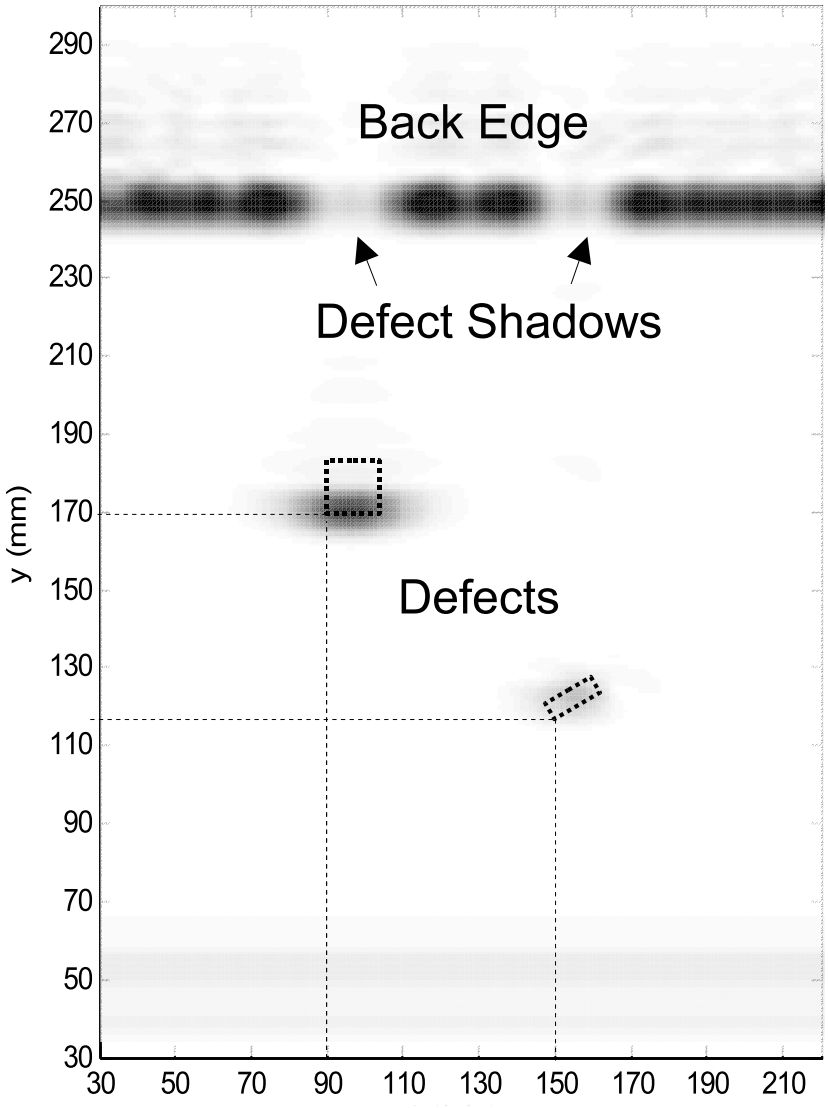

Figure 17: Results of a 3D pulse-echo inspection using a single remote sensing agent